Mon. Not. R. Astron. Soc. **000**, 1 (2007) Printed 2 February 2008 (MN LaTeX style file v2.2)

arXiv:0801.2649v1 [astro-ph] 17 Jan 2008

Extinction curves flattened by reverse shocks in supernovae

Hiroyuki Hirashita[1]*, Takaya Nozawa[2], Tsutomu T. Takeuchi[3], and Takashi Kozasa[2]

[1] *Centre for Computational Sciences, University of Tsukuba, Tsukuba 305-8577, Japan*
[2] *Department of Cosmosciences, Graduate School of Science, Hokkaido University, Sapporo 060-0810, Japan*
[3] *Institute for Advanced Research, Nagoya University, Nagoya 464-8601, Japan*

2007 December 7

ABSTRACT
We investigate the extinction curves of young galaxies in which dust is supplied from Type II supernovae (SNe II) and/or pair instability supernovae (PISNe). Since at high redshift ($z > 5$), low-mass stars cannot be dominant sources for dust grains, SNe II and PISNe, whose progenitors are massive stars with short lifetimes, should govern the dust production. Here, we theoretically investigate the extinction curves of dust produced by SNe II and PISNe, taking into account reverse shock destruction induced by collision with ambient interstellar medium. We find that the extinction curve is sensitive to the ambient gas density around a SN, since the efficiency of reverse shock destruction strongly depends on it. The destruction is particularly efficient for small-sized grains, leading to a flat extinction curve in the optical and ultraviolet wavelengths. Such a large ambient density as $n_{\rm H} \gtrsim 1$ cm^{-3} produces too flat an extinction curve to be consistent with the observed extinction curve for SDSS J1048+4637 at $z = 6.2$. Although the extinction curve is highly sensitive to the ambient density, the hypothesis that the dust is predominantly formed by SNe at $z \sim 6$ is still allowed by the current observational constraints. For further quantification, the ambient density should be obtained by some other methods. Finally we also discuss the importance of our results for observations of high-z galaxies, stressing a possibility of flat extinction curves.

Key words: dust, extinction — galaxies: evolution — galaxies: high-redshift — galaxies: ISM — supernovae: general — quasars: individual: SDSS J104845.05+463718.3

1 INTRODUCTION

Dust grains play an important role in the formation and evolution of galaxies. Dust grains control the energy balance in the interstellar medium (ISM) by absorbing stellar light and reemitting it in far infrared (FIR). Also, the surface of dust grains is a site for an efficient formation of H_2 molecules (e.g. Cazaux & Tielens 2004), which act as an effective coolant in metal-poor ISM. Those effects of dust turn on even at ~ 1% of the solar metallicity according to the calculation by Hirashita & Ferrara (2002), who argue that the star formation rate is enhanced because of the first dust enrichment in the history of galaxy evolution. The first sources of dust in the Universe are Type II (core-collapse) supernovae (SNe II) or pair instability supernovae (PISNe), since the lifetimes of their progenitors are short ($\sim 10^6$ yr). In the local Universe, dust grains are also produced by evolved low mass stars (Gehrz 1989), but this production mechanism requires much longer ($\gtrsim 1$ Gyr) timescales. The first dust supplied by SNe II or PISNe may trigger the formation of low-mass stars via dust cooling (Schneider et al. 2003; Omukai et al. 2005).

To quantify the above effects of dust in the early stages of galaxy evolution, it is crucial to know how much dust and what species of grains form in supernovae (SNe). It has been suggested by some observations of nearby SNe that dust is indeed produced in SNe, although the quantity of formed dust is still debated (e.g. Moseley et al. 1989; Dunne et al. 2003; Morgan et al. 2003; Hines et al. 2004; Sugerman et al. 2006; Meikle et al. 2007; Rho et al. 2007). By treating the nucleation and accretion in SNe, the dust composition and size distribution are theoretically calculated (Kozasa, Hasegawa, & Nomoto 1989, 1991). Recently, in order to examine the effects of dust in Population III (Pop III) objects, the formation of dust in SNe II and PISNe is extensively examined (Todini & Ferrara 2001; Nozawa et al. 2003, hereafter N03, Schneider, Ferrara, & Salvaterra 2004). The motivation for considering PISNe comes from some evidence indicating that the stars formed from metal-free gas, Population III (PopIII) stars, are very massive with a characteristic mass of a few hundred solar masses (e.g. Nakamura & Umemura 2001; Bromm & Larson 2004). Such massive stars are considered to begin pair creation of electron and positron after the helium burning phase, and finally an explosive nuclear reaction disrupts the whole stars (Fryer, Woosley, & Heger 2001; Heger & Woosley 2002). This explosion is called PISN.

---

* E-mail: hirasita@ccs.tsukuba.ac.jp

Recently, the hypothesis that the dust formation is dominated by SNe II and/or PISNe at high redshift (z) is observationally examined for some objects. We expect that at $z > 5$, when the cosmic age is less than 1 Gyr, the main sources of dust grains are SNe II and PISNe (e.g. Dwek, Galliano, & Jones 2007). Extinction curves can be used to investigate the dust properties (e.g. Mathis 1990). By using a sample of broad absorption line (BAL) quasars, Maiolino et al. (2004a) show that the extinction properties of the low-z ($z < 4$) sample is different from those of the high-z ($z > 4.9$) sample. This result is suggestive of a change in the dust production mechanism in the course of galaxy evolution. The highest-z BAL quasar in their sample, SDSS J104845.05+463718.3 (hereafter SDSS J1048+4637) at $z = 6.2$ shows an extinction curve flat at wavelength $\lambda \gtrsim 1700$ Å and rising at $\lambda \lesssim 1700$ Å. Maiolino et al. (2004b) show that the extinction curve of SDSS J1048+4637 is in excellent agreement with the SN II dust models by Todini & Ferrara (2001). Bianchi & Schneider (2007) consider dust destruction by reverse shock in SNe, suggesting that 2–20% of the initial dust mass survives, and that the extinction curve after the destruction is still consistent with that of SDSS J1048+4637. More recently, Stratta et al. (2007) show that the dust extinction in the host galaxy of GRB 050904 at $z = 6.3$ can be explained by the extinction curve of SDSS J1048+4637, further supporting that the SNe II are the main sources of dust at $z > 6$. Also, Willott et al. (2007) find a similar extinction property for CFHQS J1509-1749 ($z = 6.12$) to that of SDSS J1048+4637.

There are other series of theoretical papers on the extinction curves of high-z objects. Hirashita et al. (2005, hereafter H05) calculate the extinction curve based on the dust production calculation by N03. They also reproduce the extinction curve of SDSS J1048+4637 by using the the dust production in SNe II, although the dust composition and size distribution are different from those of Todini & Ferrara (2001). Recently, Nozawa et al. (2007, hereafter N07) have treated the dust destruction by the reverse shock as done by Bianchi & Schneider (2007), but considering the motion of dust relative to gas caused by the drag force and the destruction of dust in the radiative phase as well as in the non-radiative phase of supernova remnants. Then, they show that the size distribution of grains supplied in the ISM is strongly modified by the reverse shock. Grains smaller than ~ 0.02 μm are efficiently destroyed if the ambient hydrogen number density is larger than 0.1 cm^{-3}. Thus, it is important to reexamine the consistency between the observed extinction curve and the reverse shock destruction.

In this paper, we calculate the extinction curves based on the dust properties calculated by N07, who have focused on the effect of reverse shock destruction in SNe. Then, we compare the results with observed extinction curves at high z. This paper is organized as follows. First, we describe our theoretical treatment to calculate the extinction curves of SN II and PISN dust in Section 2. We show and examine our results in Section 3. We discuss our results from the observational viewpoint in Section 4, and finally give the conclusion of this paper in Section 5.

2 MODEL

We derive the theoretical extinction curves of dust grains produced in SNe II and PISNe and subsequently destroyed by the reverse shock. Those grains are considered to be supplied in the interstellar spaces. The grain composition and size distribution in SNe before the destruction is calculated by N03, whose results are adopted as the initial conditions for the calculations of reverse shock destruction by N07. By using the results by N07, the extinction curves are calculated by the same method as in H05. The outline of our calculation is reviewed as follows.

Table 1. Summary of grain species.

Species	condition^a	Ref^b	density (δ_j) (g cm^{-3})
C	u	1	2.28
Si	u	2	2.34
SiO_2	m/u	3	2.66
Fe	u	4	7.95
FeS	u	4	4.87
Fe_3O_4	m	5	5.25
Al_2O_3	m/u	6	4.01
MgO	u	7	3.59
$MgSiO_3$	m/u	8	3.20
Mg_2SiO_4	m/u	4	3.23

[a] The classifications "m", "u", and "m/u" mean that the species is formed in mixed, unmixed, and both supernovae, respectively.

[b] References for optical constants: (1) Edo (1983); (2) Piller (1985); (3) Philipp (1985); (4) Semenov et al. (2003); (5) A. Triaud and H. Mutschke (2006 private communication and see http://www.astro.uni-jena.de/Laboratory/OCDB/oxsul.html); (6) Toon, Pollack, & Khare (1976); (7) Roessler & Huffman (1991); (8) Semenov et al. (2003) (The optical constants of Mg_2SiO_4 are used for $\lambda \leqslant 0.3$ μm).

2.1 Dust production and destruction in SNe II and PISNe

N03 calculate the dust composition and size distribution in the ejecta of PopIII SNe II and PISNe based on the supernova model of Umeda & Nomoto (2002), carefully treating the radial density profile and the temperature evolution. As mentioned in H05, the resulting grain composition and size distribution are not sensitive to the metallicity of progenitor (N03). Thus, the assumption of zero-metallicity is not essential in this paper, and our results can be applicable to metal-enriched systems. Since it is still uncertain how efficiently the mixing of atoms within SNe occurs, N03 treat two extreme cases for the mixing of elements: one is the *unmixed* case in which the original onion-like structure of elements is preserved, and the other is the *mixed* case in which the elements are uniformly mixed within the helium core. They show that the formed dust species depend largely on the mixing of seed elements within SNe, because the dominant reactions change depending on the ratio of available elements. The formed grain species in the calculation of N03 are listed in Table 1.

In the unmixed ejecta, a variety of grain species (Si, Fe, Mg_2SiO_4, $MgSiO_3$, MgO, Al_2O_3, SiO_2, FeS, and C) condense, while in the mixed ejecta, only oxide grains (SiO_2, $MgSiO_3$, Mg_2SiO_4, Al_2O_3, and Fe_3O_4) form. The species are summarized in Table 1. Based on the results in N03, N07 treat the dust destruction by the reverse shock in the supernova remnant. They find that small-sized grains suffer dust destruction by the reverse shock and that the final grain size distribution is biased to larger grains than the original distribution calculated by N03. We adopt their results as the properties of grains supplied to the interstellar space. Following H05, we adopt the representative progenitor mass of SNe II as 20 $M_\odot$ and that of PISNe as 170 $M_\odot$. We also investigate the mixed and unmixed cases. Therefore, we treat four cases:

(a) mixed SNe II;
(b) unmixed SNe II;
(c) mixed PISNe; and
(d) unmixed PISNe.
All the formulation and the results can be seen in N03 and N07. The grains are assumed to be homogeneous and spherical.

2.2 Optical constants and extinction curves

In order to calculate extinction curves, the optical constants of grains are necessary. We adopt the references listed in Table 1 for the optical constants. Here, we only explain the difference from H05. The optical constants are updated for Fe_3O_4. For $MgSiO_3$, we adopt the optical constants of Mg_2SiO_4 at $\lambda \leqslant 0.3$ μm, where the currently available experimental data are relatively poor (Dorschner et al. 1995). For Si and SiO_2, we adopt the optical constants for amorphous instead of crystal since the grains rapidly grow in SNe. Subsequent sputtering due to the reverse shock may also tend to destroy crystal structures and to form more complicated amorphous solids. The infrared broad feature at $\lambda \simeq 21$ μm is also better explained by amorphous SiO_2 than by crystal SiO_2 (Rho et al. 2007). We discuss the uncertainty in the assumed optical constants in Appendix A.

By using those optical constants, we calculate the absorption and scattering cross sections of homogeneous spherical grains with various sizes based on the Mie theory (Bohren & Huffman 1983). Then, the opacity of grain j (j denotes a grain species) as a function of wavelength, $\tau_{\lambda,\,j}$, is calculated by weighting the cross sections according to the size distribution. The extinction curve is presented in the form of A_λ/A_{λ_0} (A_λ is the extinction in units of magnitude at wavelength λ, and λ_0 is a reference wavelength). The extinction in units of magnitude is proportional to the optical depth as $A_{\lambda,\,j} = 1.086\tau_{\lambda,\,j}$, where $A_{\lambda,\,j}$ is the extinction of species j in units of magnitude as a function of λ. The total extinction A_λ is calculated by summing $A_{\lambda,\,j}$ for all the concerning species:

$$A_\lambda = \sum_j A_{\lambda,\,j}\,. \tag{1}$$

For more details, see H05. Since we normalize the extinction at a certain wavelength λ_0, only relative values of $\tau_{\lambda,\,j}$ are important.

3 RESULTS

3.1 Extinction curves after the reverse shock destruction

As shown in N07, the final size distribution of grains after the reverse shock destruction is sensitive to the density of the ambient ISM. Here we start from the results for $n_{\rm H} = 1$ cm^{-3}, where $n_{\rm H}$ is the hydrogen number density in the ambient medium, to examine the effect of grain destruction on the extinction curve. In Figure 1, we show the resulting extinction curves of the four cases in Section 2.1. The contribution of each species is also shown. We normalize the extinction to A_V (i.e., $\lambda_0 = 0.55$ μm).

The extinction curves of dust produced by the mixed SNe II and PISNe are dominated by SiO_2 (Figures 1a and c; in the PISN case, only the contribution from SiO_2 appears and the total extinction curve is identical to the extinction curve of SiO_2). The extinction curve is flatter than that without destruction because the reverse shock efficiently destroys small grains and the mean grain size becomes larger.

The extinction curve for the unmixed SNe II (Figure 1b) is dominated by Si and C. However, as shown in H05, the extinction curve without reverse shock destruction is dominated by Mg_2SiO_4 and FeS for $\lambda \lesssim 0.5$ μm and by Si for $\lambda \gtrsim 0.5$ μm. Since Si and C grains are larger than the other species, they survive the reverse shock more than the others. For the same reason, the extinction curve of unmixed PISNe is dominated by Si. Also for the unmixed SNe II and PISNe, the extinction curves of grains after the reverse shock destruction are flatter, since small-sized grains are selectively destroyed and the mean size of the grains becomes large.

3.2 Dependence on the ambient medium density

As shown by N07, the efficiency of the reverse shock destruction is sensitive to the density of the ambient medium. Here we investigate the variation of the extinction curve for various ambient densities. N07 have examined three cases for the ambient hydrogen number density: $n_{\rm H} = 0.1$, 1, and 10 cm^{-3}. N07 show that the grains are almost completely destroyed for $n_{\rm H} = 10$ cm^{-3}. Thus, we calculate the cases for $n_{\rm H} = 0.1$ and 1 cm^{-3}. For comparison, we also show the results without the reverse shock destruction (this case is called non-destruction case). For the details for the non-destruction case, see N03 and H05. The results are shown in Figure 2. As expected, the extinction curve becomes flatter for a larger ambient density because the destruction efficiency of small-sized grains is larger. In Section 4, our results are compared with high-z data of extinction curve.

Bianchi & Schneider (2007) also state that the extinction curve becomes flatter, although they start from a different dust formation model based on Todini & Ferrara (2001). The differences between Bianchi & Schneider (2007) and the present work are partly due to the differences in optical constants: amorphous carbon is responsible for most of the extinction in their work. Furthermore, their results show more survival of small grains than those of N07. As mentioned in N07, the difference comes from the treatment of grain motion: In N07, the trap of grains in a hot and dense zone between forward and reverse shocks is properly treated, and this effect enhances the destruction of small-sized grains. Thus, our results show flatter extinction curves than those of Bianchi & Schneider (2007) especially when the ambient gas density is large.

4 OBSERVATIONAL DISCUSSION

4.1 Comparison with high-z data

H05 show that the dust production model of the unmixed SNe II in N03 is consistent with the extinction curve of SDSS J1048+4637. However, it is crucial to compare our new results including the reverse shock destruction with SDSS J1048+4637. In particular, we may obtain constraints on the ambient gas density as well as the progenitors. We compare our results with the restframe UV extinction curve of SDSS J1048+4637. The plausible range derived by Maiolino et al. (2004b) is shown by the shaded areas in Figure 3.

In each panel of Figure 3, we show the theoretical extinction curves calculated for various ambient hydrogen number densities (same as Figure 2 but normalized to the extinction at $\lambda = 0.3$ μm, i.e., $\lambda_0 = 0.3$ μm). We also show the results of the non-destruction case. Because of the variation caused by the destruction, various types of progenitors may be allowed. For example, the mixed SNe II are consistent with the observed extinction curve if $n_{\rm H} \sim 1$ cm^{-3}. In all cases, the ambient number density $n_{\rm H} \gtrsim 1$ cm^{-3} produces too flat extinction curves to be consistent with the data.

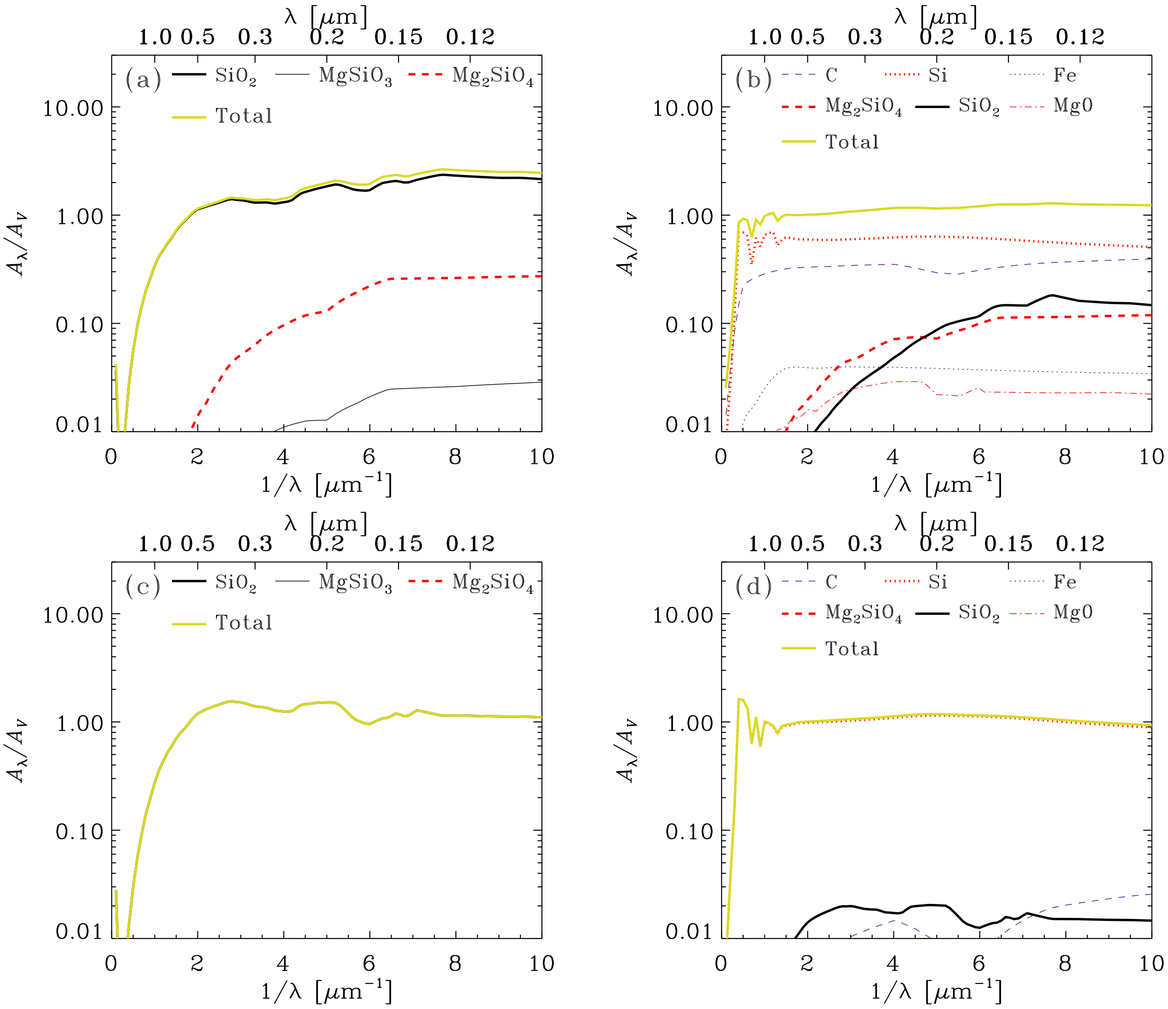

Figure 1. Extinction curves of grains produced in (a) the mixed ejecta with the progenitor of 20 $M_\odot$, (b) the unmixed ejecta with the progenitor of 20 $M_\odot$, (c) the mixed ejecta with the progenitor of 170 $M_\odot$, and (d) the unmixed ejecta with the progenitor of 170 $M_\odot$. The ambient hydrogen number density is assumed to be $n_\mathrm{H} = 1$ cm^{-3}. The extinction is normalized to the value at $\lambda = 0.55$ μm. The correspondence between the species and the lines is shown in each panel. Note that some of the species are almost completely destroyed and do not appear on the figures and that in Panel (c), only SiO$_2$ contributes to the total extinction curve.

4.2 Ambient density around SNe

In the previous subsection, we have shown that the extinction curves are sensitive to the ambient density of SNe. Thus, it is important to constrain the density first. Unfortunately, there is no direct observational constraint on the gas density in SDSS J1048+4637.

It is rather interesting to point out that the extinction curves for $n_\mathrm{H} \lesssim 0.1$ cm^{-3} of the unmixed SNe II is quite consistent with the extinction curves of SDSS J1048+4637. The mixed SNe II also reproduce the observational extinction curve quite well if the ambient hydrogen number density is ~ 1 cm^{-3}. The extinction curves of PISNe are too flat for $n_\mathrm{H} \gtrsim 1$ cm^{-3}. Considering the uncertainty in the observational data, however, the extinction curves of PISNe are not rejected for $n_\mathrm{H} \sim 0.1$–1 cm^{-3}.

Theoretically, it is possible to examine the density evolution around the progenitors of SNe. Kitayama et al. (2004) show that in small objects whose typical halo mass is $\sim 10^6$ $M_\odot$, the entire gas cloud is completely swept by the ionization front, and the dynamical expansion of the ionized region reduces the ambient density down to $n_\mathrm{H} \lesssim 1$ cm^{-3}. On the contrary, in more massive objects, the evacuation of the gas around a massive star does not efficiently occur and the final gas density is much higher. However, if we consider 3-dimensional complex structure of interstellar medium, the density around a massive star is hard to predict theoretically. Thus, at this moment, a direct constraint on the gas density in SDSS J1048+4637 by using for example excitation states of molecular or atomic lines is desired.

In summary, the current observational extinction curve at $z \sim 6$ can be explained by the hypothesis that dust is produced by SNe II and/or PISNe and destroyed subsequently by reverse shocks. In addition, the results in this paper newly propose that the ambient density should be less than ~ 1 cm^{-3}, since the reverse shock destruction flattens the extinction curve too much if $n_\mathrm{H} \gtrsim 1$ cm^{-3}.

4.3 Flat extinction curves at high z?

As shown in Section 3, a flat extinction curve is naturally produced by reverse shock destruction in SNe. At $z > 5$, where it is probable that SNe II or PISNe predominantly supply dust grains, it is worth investigating possibility that extinction curves are flat.

Indeed, there are some pieces of supporting evidence for flat

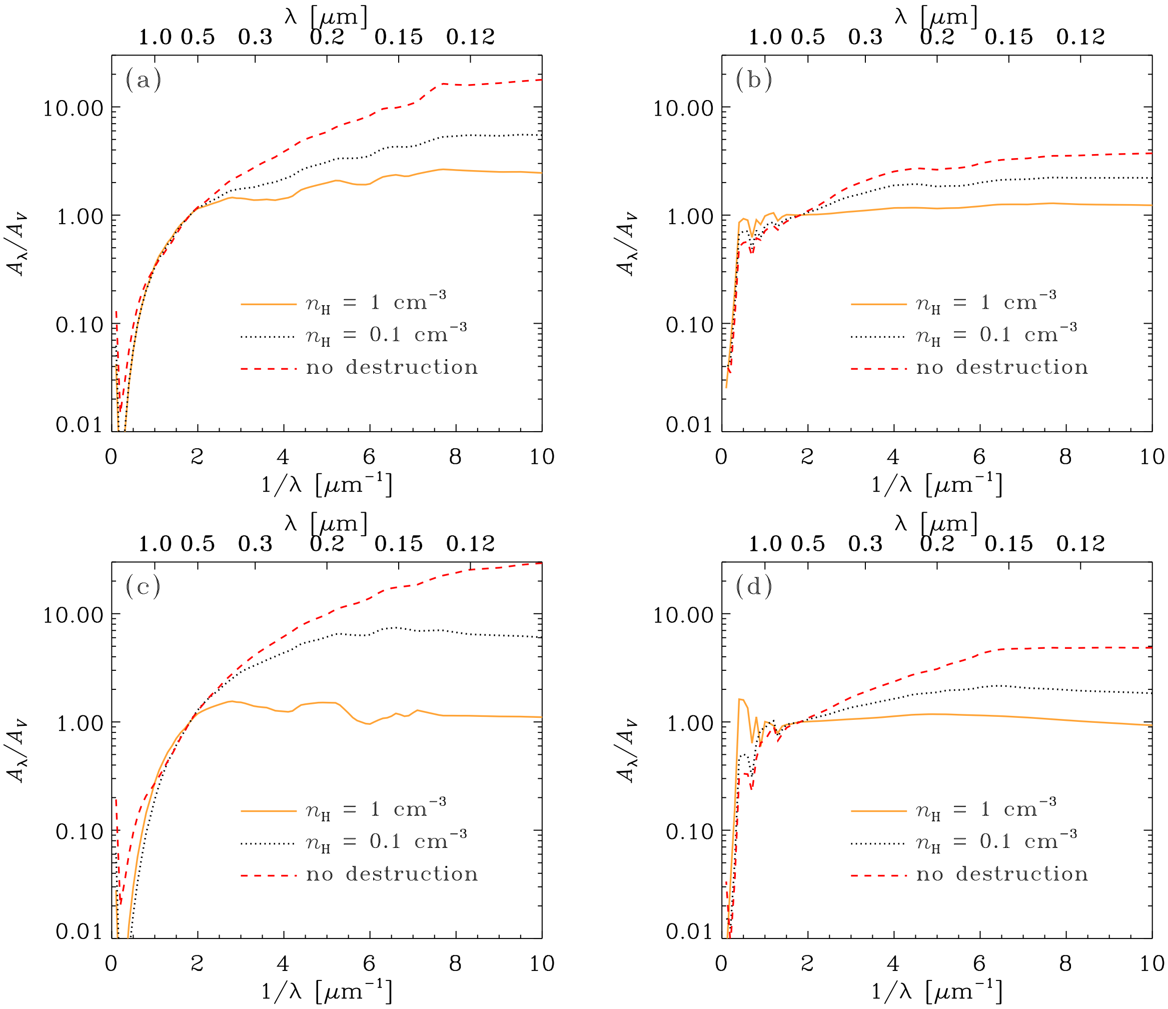

Figure 2. Extinction curves of grains for various ambient hydrogen number densities ($n_{\rm H} = 1$ and 0.1 cm^{-3} for the solid and dashed lines, respectively). The case without the reverse shock destruction (non-destruction case) is also shown in each panel (the dashed line). The progenitor model in each panel is the same as that in Figure 1.

extinction curves at $z > 5$. Among the sample in Maiolino et al. (2004a), two BAL quasars, SDSS J1044−0125 at $z = 5.8$ and SDSS J0756+4104 at $z = 5.1$, show no reddening but are detected at sub-mm (Priddey et al. 2003). The sub-mm observations yield dust masses in the range $10^{8-9}\ M_\odot$ for those two quasars. The absence of reddening and the presence of sub-mm emission (dust emission) may be contradictory, but they are consistent if we assume a flat extinction curve. An extremely small reddening of a BAL quasar SDSS 1605−0112 at $z = 4.9$ (Maiolino et al. 2004a) may also be attributed to a flat extinction curve. In the future, extinction curves of high-z sub-mm samples (Bertoldi et al. 2003; Priddey et al. 2003; Robson et al. 2004; Beelen et al. 2006) in comparison with theoretical modeling of sub-mm emission (e.g. Takeuchi et al. 2003, 2005) enable us to further investigate the properties and origins of dust grains in the early Universe.

Also at lower z ($\lesssim 5$), it may be worth to consider possibility of flat extinction curves. Direct indications of dust at $z \lesssim 5$ come, for example, from the reddening of background quasars (Fall et al. 1989; Zuo et al. 1997). The depletion of heavy elements in quasar absorption line systems, especially damped Lyα clouds (DLAs), also supports the presence of dust in distant systems (e.g. Pettini et al. 1994; Vladilo 2002; Ledoux et al. 2003). However, there are some observational results that show no significant reddening of DLAs (Murphy & Liske 2004; Ellison, Hall, & Lira 2005). The flat extinction curve proposed above has importance that the lack of reddening does not necessarily mean the absence of dust. Other than DLAs, some objects whose extinction curves are derived by gamma-ray bursts (Chen, Li, & Wei 2006) or by gravitational lensing (e.g. Falco et al. 1999; Muñoz et al. 2004) seem to have a flat extinction curve in UV.

4.4 Possibility of subsequent steepening

Dust grains supplied into interstellar spaces suffer various processes that modify their size distribution. One of such processes is the destruction by forward shocks of supernova remnants. The dust destruction by forward shocks has already been examined by Nozawa, Kozasa, & Habe (2006). Here we have examined the effect of forward shock destruction and have confirmed that one passage of a supernova forward shock has negligible influence on the extinction curve. This is because after an efficient sputtering in supernova remnants the opacity is already dominated by large grains which are hard to destroy. However, shattering may increase the number of small-size grains (Borkowski & Dwek

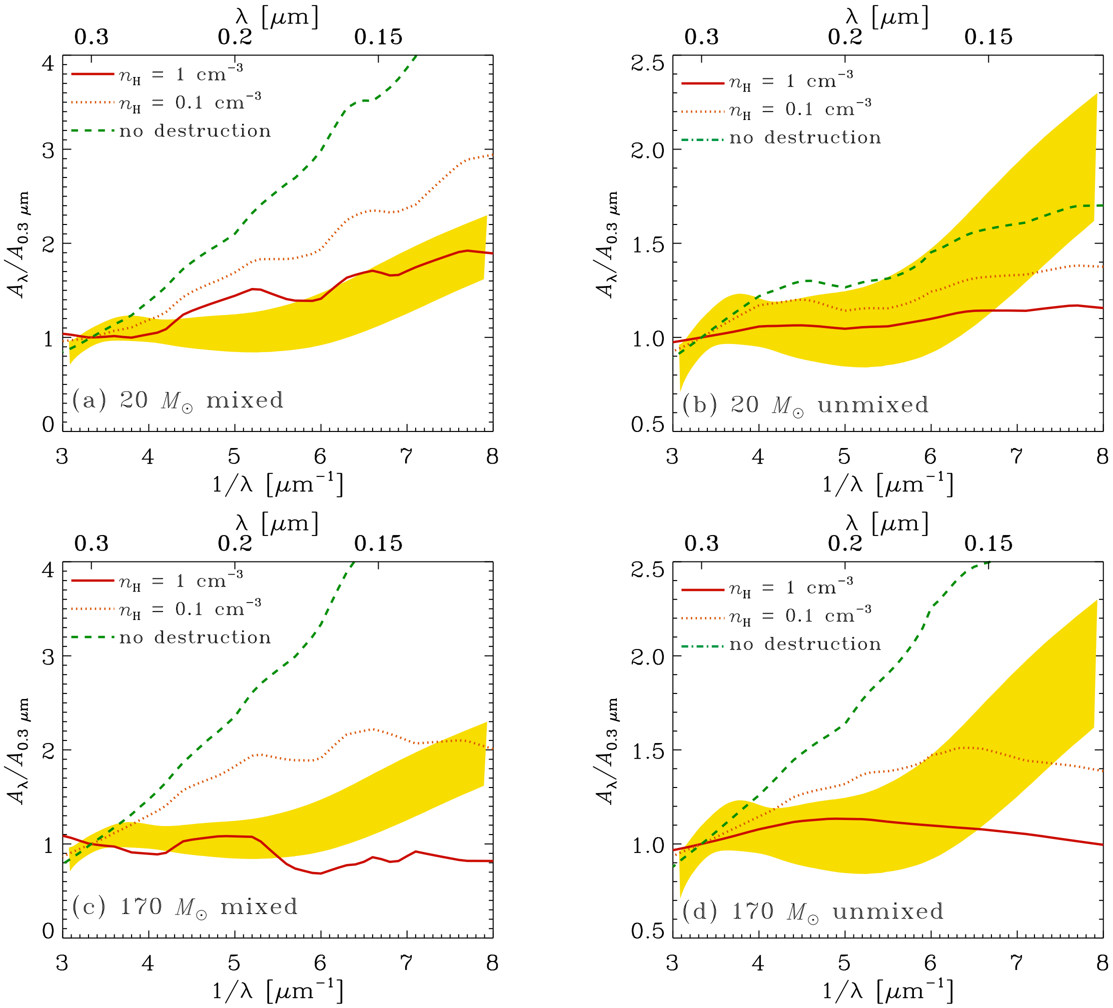

Figure 3. Extinction curves normalized at $\lambda = 0.3$ μm. The same theoretical curves as those in Figure 2 are plotted. The shaded area in each panel show the range observationally derived by Maiolino et al. (2004b) for SDSS J1048+4637 at $z = 6.2$.

1995; Jones, Tielens, & Hollenbach 1996), steepening the extinction curve. Quantitative study of the effect of shattering on the extinction curve is left for future work.

5 CONCLUSION

We have theoretically investigated the extinction curves of grains produced in SNe II and PISNe. Since at high $z(> 5)$, low-mass stars cannot be dominant sources for dust grains, SNe II and PISNe, whose progenitors are massive stars with short lifetimes, can govern the dust production. While our previous works (N03 and H05) did not consider the reverse shock destruction induced by a collision with ambient interstellar medium, we adopt the composition and size distribution of grains of N07, who take into account the reverse shock destruction.

We have found that the extinction curve is sensitive to the ambient gas density around SNe, since the efficiency of reverse shock destruction is largely dependent on it. The destruction is significant for small-sized grains, leading to a flat extinction curve in the optical and UV. Such a large ambient density as $n_{\rm H} \gtrsim 1$ cm^{-3} produces too flat an extinction curve to be consistent with the observed extinction curve for SDSS J1048+4637 at $z = 6.2$. Although the extinction curve is highly sensitive to the ambient density, the hypothesis that the dust is predominantly formed by SNe at $z \sim 6$ is still allowed if $n_{\rm H}$ is smaller than 1 cm^{-3}. For further quantification, the ambient density should be constrained by some other methods.

It is worth noting that a flat extinction curve produced by effective reverse shock destruction may explain the absence of reddening of systems in which dust is known to be present by far-infrared/sub-mm emission or by depletion of heavy elements.

ACKNOWLEDGMENTS

We thank R. Maiolino and his collaborators for kindly providing us with their data on the extinction curve of SDSS J1048+4637. We are also grateful to S. Bianchi for helpful comments that improved this paper very much. HH has been supported by Grants-in-Aid for Scientific Research of the Ministry of Education, Culture, Sports, Science and Technology (MEXT) of Japan (Nos. 18026002 and 18740097). TN also has been supported by the same grants (Nos. 18104003 and 19740094). TTT has been supported by the Special Coordination Funds for Promotion Science and Technology (SCF) commissioned by the MEXT (MEXT) of Japan. We fully utilized the NASA's Astrophysics Data System Abstract Service (ADS).

REFERENCES

Beelen, A., Cox, P., Benford, D. J., Dowell, C. D., Kovács, A., Bertoldi, F., Omont, A., & Carilli, C. L. 2006, ApJ, 642, 694

Bertoldi, F., Carilli, C. L., Cox, P., Fan, X., Strauss, M. A., Beelen, A., Omont, A., & Zylka, R. 2003, A&A, 406, L55

Bianchi, S., & Schneider, R. 2007, MNRAS, 378, 973

Bohren, C. F., & Huffman, D. R. 1983, Absorption and Scattering of Light by Small Particles (New York: Wiley)

Borkowski, K. J., & Dwek, E. 1995, ApJ, 454, 254

Bromm, V., & Larson, R. B. 2004, ARA&A, 42, 79

Cazaux, S., Tielens, A. G. G. M. 2004, ApJ, 604, 222

Chen, S. L., Li, A., & Wei, D. M. 2006, ApJ, 647, L13

Dorschner, J., Begemann, B., Henning, Th., Jaeger, C., & Mutschke, H. 1995, A&A, 300, 503

Dunne, L., Eales, S., Ivison, R., Morgan, H., & Edmunds, M. 2003, Nat, 424, 285

Dwek, E., Galliano, F., & Jones, A. P. 2007, ApJ, 662, 927

Edo, O. 1983, PhD Dissertation, Dept. of Physics, University of Arizona

Edward, D. F. 1985, in Handbook of Optical Constants of Solids ed. E. D. Palik, Academic Press, San Diego, USA p. 547

Ellison, S. L., Hall, P. B., & Lira, P. 2005, AJ, 130, 1345

Falco, E. E., et al. 1999, ApJ, 523, 617

Fall, S. M, Pei, Y. C. & McMahon, R. G. 1989, ApJ, 341, L5

Fryer, C. K., Woosley, S. E., & Heger, A. 2001, ApJ, 550, 372

Gehrz, R. D. 1989, in Allamandola L. J., Tielens A. G. G. M., eds, Proc. IAU Symp. 135, Interstellar Dust, Kluwer, Dordrecht, p. 445

Heger, A., & Woosley, S. E. 2002, ApJ, 567, 532

Hines, D. C., et al. 2004, ApJS, 154, 290

Hirashita, H., & Ferrara, A. 2002, MNRAS, 337, 921

Hirashita, H., Nozawa, T., Kozasa, T., Ishii, T. T., & Takeuchi, T. T. 2005, MNRAS, 357, 1077 (H05)

Jones, A. P., Tielens, A. G. G. M., & Hollenbach, D. J. 1996, ApJ, 469, 740

Kitayama, T., Yoshida, N., Susa, H., & Umemura, M. 2004, ApJ, 613, 631

Kozasa, T., Hasegawa, H., & Nomoto, K. 1989, ApJ, 344, 325

Kozasa, T., Hasegawa, H., & Nomoto, K. 1991, A&A, 249, 474

Ledoux, C., Petitjean, P., & Srianand, R. 2003, MNRAS, 346, 209

Maiolino, R., Oliva, E., Ghinassi, F., Pedani, M., Mannucci, F., Mujica, R., Juarez, & Y. 2004a, A&A, 420, 889

Maiolino, R., Schneider, R., Oliva, E., Bianchi, S., Ferrara, A., Mannucci, F., Pedani, M., & Roca Sogorb, M. 2004b, Nat, 431, 533

Mathis, J. S. 1990, ARA&A, 28, 37

Meikle, W. P. S., et al. 2007, ApJ, 665, 608

Morgan, H. L., Dunne, L., Eales, S. A., Ivison, R. J., & Edmunds, M. G. 2003, ApJ, 597, L33

Moseley, S. H., Dwek, E., Glaccum, W., Graham, J. R., & Loewenstein, R. F. 1989, Nature, 340, 697

Muñoz, J., A., Falco, E. E., Kochanek, C. S., McLeod, B. A., & Mediavilla, E. 2004, ApJ, 605, 614

Murphy, M. T., & Liske, J. 2004, MNRAS, 354, L31

Nakamura, F., & Umemura, M. 2001, ApJ, 548, 19

Nozawa, T., Kozasa, T., & Habe, A. 2006, ApJ, 648, 435

Nozawa, T., Kozasa, T., Umeda, H., Maeda, K., & Nomoto, K. 2003, ApJ, 598, 785 (N03)

Nozawa, T., Kozasa, T., Habe, A., Dwek, E., Umeda, H., Tominaga, N., Maeda, K., & Nomoto, K. 2007, ApJ, 666, 955 (N07)

Omukai, K., Tsuribe, T., Schneider, R., & Ferrara, A. 2005, ApJ, 626, 627

Pettini, M. H., Smith, L. J., Hunstead, R. W., & King, D. L. 1994, ApJ, 426, 79

Philipp, H. R. 1985, in Handbook of Optical Constants of Solids, ed. E. D. Palik, Academic Press, San Diego, p. 719

Piller, H. 1985, in Handbook of Optical Constants of Solids, ed. E. D. Palik, Academic Press, San Diego, p. 571

Priddey, R. S., Isaak, K. G., McMahon, R. G., Robson, E. I., Pearson, C. P. 2003, MNRAS, 344, L74

Rho, J., Kozasa, T., Reach, W. T., Smith, J. D., Rudnick, L., DeLaney, T., Ennis, J. A., Gomez, H., & Tappe, A. 2007, ApJ, in press (arXiv:0709.2880)

Robson, I., Priddey, R. S., Isaak, K. G., & McMahon, R. G. 2004, MNRAS, 351, L29

Roessler, D. M., & Huffman, D. R. 1991, in Handbook of Optical Constants of Solids II, ed. E. D. Palik, Academic Press, San Diego, p. 919

Schneider, R., Ferrara, A., & Salvaterra, R. 2004, MNRAS, 351, 1379

Schneider, R., Ferrara, A., Salvaterra, R., Omukai, K., & Bromm, V. 2003, Nature, 422, 869

Semenov, D., Henning, Th., Helling, Ch., Ilgner, M., & Sedlmayr, E. 2003, A&A, 410, 611

Stratta, G., Maiolino, R., Fiore, F., & D'Elia, V. 2007, ApJ, 661, L9

Sugerman, B. E. K., et al. 2006, Science, 313, 196

Takeuchi, T. T., Hirashita, H., Ishii, T. T., Hunt, L. K., & Ferrara, A. 2003, MNRAS, 43, 839

Takeuchi, T. T., Ishii, T. T., Nozawa, T., Kozasa, T., & Hirashita, H. 2005, MNRAS, 362, 592

Todini, P., & Ferrara, A. 2001, MNRAS, 325, 726

Toon, O. B., Pollack, J. B., & Khare, B. N. 1976, J. Geophys. Res., 81, 5733

Umeda, H., & Nomoto, K. 2002, ApJ, 565, 385

Vladilo, G. 2002, A&A, 391, 407

Willott, C. J., et al. 2007, AJ, 134, 2435

Zuo, L., Beaver, E. A., Burbidge, E. M., Cohen, R. D., Junkkarinen, V. T., & Lyons, R. W. 1997, ApJ, 477, 568

APPENDIX A: COMPARISON BETWEEN CRYSTAL AND AMORPHOUS GRAINS

As mentioned in Section 2.2, the optical constants of crystal Si and SiO_2 are available, while we have used those of amorphous Si and SiO_2. Since those species dominate the extinction curves, it is important to examine the uncertainty caused by assumed material states. The optical constants of crystal Si and SiO_2 are taken from Edward (1985) and Philipp (1985), respectively. As a representative, we examine the case of $n_{\rm H} = 1$ cm^{-3}. In the mixed and unmixed cases, the difference between crystal and amorphous are examined for the dominant species, SiO_2 and Si, respectively.

In Figures A1a and b, we show the extinction curves with the progenitor masses of 20 $M_\odot$ and 170 $M_\odot$, respectively, for the mixed supernovae. From those figures, we observe that the overall trend is similar between the two species of SiO_2. Thus we conclude

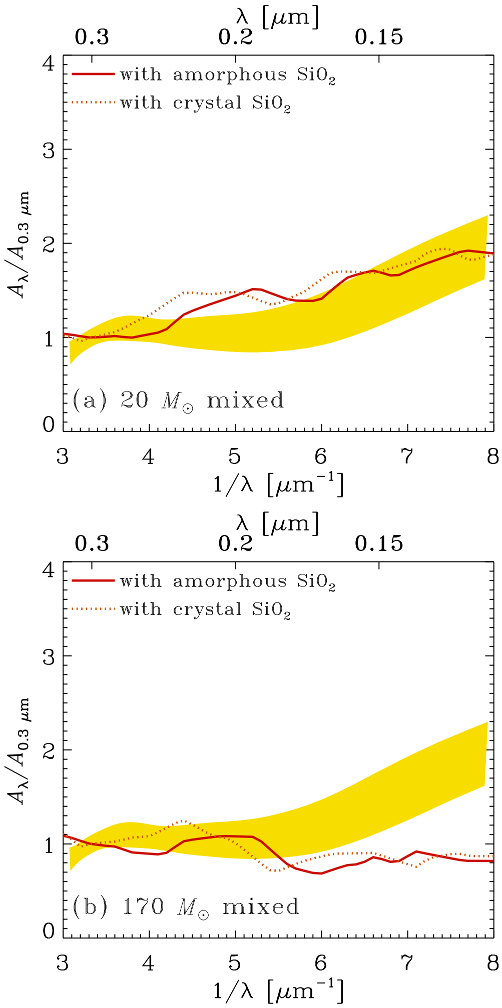

Figure A1. The same as Figure 3 for the mixed SN II and PISN for $n_H = 1$ cm^{-3} (solid lines in panels a and b, respectively). For SiO_2, we adopt the optical constants of amorphous and crystal solids for the solid and dotted lines. For other species, the same optical constants as those in Figure 3 are applied.

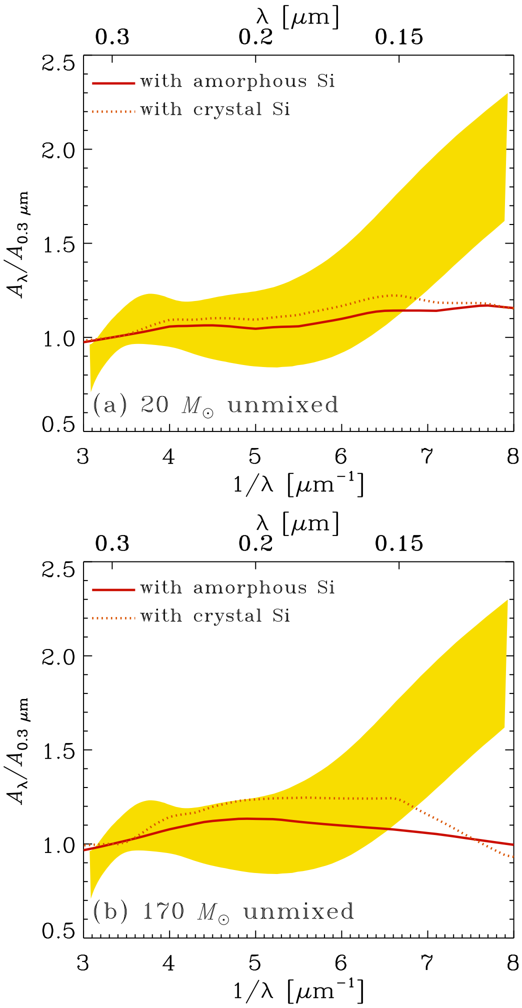

Figure A2. The same as Figure 3 for the unmixed SN II and PISN for $n_H = 1$ cm^{-3} (solid lines in panels a and b, respectively). For Si, we adopt the optical constants of amorphous and crystal solids for the solid and dotted lines. For other species, the same optical constants as those in Figure 3 are applied.

that the two species of SiO_2 are indistinguishable in the extinction curve within the uncertainty in the current observational data.

In Figure A2, we make the same kind of comparison for unmixed SNe, but the difference between crystal and amorphous species is examined for Si. As can be seen from the figure, the difference is smaller than the uncertainty in the observational data.